Kinetic-structural analysis of neuronal growth cone veil motility

Anne K. Mongiu*, Elizabeth L. Weitzke, Oleg Y. Chaga and Gary G. Borisy‡

Department of Cell and Molecular Biology, Northwestern University Feinberg School of Medicine, and Marine Biological Laboratory, 303 E. Chicago Avenue, Chicago, IL 60611, USA

*Author for correspondence (e-mail: akmongi@northwestern.edu)
‡Present address: MBL, 7 Water Street, Woods Hole, MA 02543, USA

Summary

Neuronal growth cone advance was investigated by correlative light and electron microscopy carried out on chick dorsal root ganglion cells. Advance was analyzed in terms of the two principal organelles responsible for protrusive motility in the growth cone – namely, veils and filopodia. Veils alternated between rapid phases of protrusion and retraction. Electron microscopy revealed characteristic structural differences between the phases. Our results provide a significant advance in three respects: first, protruding veils are comprised of a densely branched network of actin filaments that is lamellipodial in appearance and includes the Arp2/3 complex. On the basis of this structural and biomarker evidence, we infer that the dendritic nucleation and/or array-treadmilling mechanism of protrusive motility is conserved in veil protrusion of growth cones as in the motility of fibroblasts; second,

retracting veils lack dendritic organization but contain a sparse network of long filaments; and third, growth cone filopodia have the capacity to nucleate dendritic networks along their length, a property consistent with veil formation seen at the light microscopic level but not previously understood in supramolecular terms. These elements of veil and filopodial organization, when taken together, provide a conceptual framework for understanding the structural basis of growth cone advance.

Introduction

The elongation and path finding of neurons depend upon the motility and sensory properties residing within a terminal specialization of cytoplasm known as the growth cone (Harrison, 1910; Landis, 1983). The motility behavior and cytomechanical properties of growth cones have been extensively investigated (Argiro et al., 1984; Heidemann et al., 1990; Suter and Forscher, 2000) and the molecular pathways by which they respond to environmental signals have been substantially unraveled (Gallo and Letourneau, 2004; Henley and Poo, 2004; Kalil and Dent, 2005; Luo, 2002). The relationship of lamellar extensions to shaft adhesions has been investigated (Steketee and Tosney, 2002). However, the supramolecular structure underlying dynamic growth cone motility has not been clearly delineated – especially in relationship to its temporal behavior. Understanding the structure and dynamics of the cytoskeletal apparatus within the growth cone is important for learning how the signaling pathways connect to the motility machinery, which in turn determines how growth cones are directed to developmental targets.

Growth cone advance has been described in terms of the behavior of two principal modes of actin filament organization – lamellipodia and filopodia – which are frequently referred to as veils and microspikes, respectively, in the neuronal literature (Bray and Hollenbeck, 1988; Dent and Gertler, 2003). In general, net advance of the growth cone occurs by cycles of

protrusion and retraction (Bray and Chapman, 1985), much as was originally described for fibroblasts (Abercrombie et al., 1970; Abercrombie et al., 1971). Investigations of the large growth cone of Aplysia neurons led to the formulation that the growth cone could be divided into three structural domains: the microtubule-rich central domain, the peripheral actin-rich domain, and the transitional domain situated in between the two, where there is overlap of microtubules and actin structures (Bridgman and Dailey, 1989; Forscher and Smith, 1988; Smith, 1988). The actin-rich peripheral domain contains the long actin filaments bundled into radial microspikes (filopodia) interspersed with a meshwork of veil or lamellipodial actin filaments (Lewis and Bridgman, 1992; Tosney and Wessells, 1983; Yamada et al., 1970; Yamada et al., 1971).

One question, which is as yet unanswered, is whether or not growth cone and fibroblast lamellipodia advance by similar or distinctive mechanisms. In non-neuronal cells, lamellipodial protrusion has been accounted for by an Arp2/3-dependent, dendritic nucleation/array treadmilling mechanism (Pollard and Borisy, 2003; Bernheim-Groswasser et al., 2002). However, recent publications have called into question whether neuronal advance proceeds by an Arp2/3-dependent mechanism and have raised the possibility that additional Arp2/3 independent mechanisms may exist. Genetic experiments generating null alleles for the Scar-Wasp-Arp pathway in the mushroom body neurons of *Drosophila* provided evidence that the Arp2/3 complex was not essential

for axon growth in vivo (Ng and Luo, 2004). A similar conclusion was drawn for hippocampal neurons in culture in which Arp2/3 function had been diminished by expression of a dominant negative construct (Strasser et al., 2004). In both studies, although axon outgrowth occurred, pathfinding was aberrant.

The conclusion that the Arp2/3 complex is not essential for axon outgrowth is consistent with an older literature demonstrating that, under sufficiently adhesive conditions, actin polymerization itself is not essential for neurite outgrowth (Marsh and Letourneau, 1984). Further, path-finding in situ was disoriented in growth cones that had been subjected to cytochalasin treatment (Bentley and Toroian-Raymond, 1986; Chien et al., 1993). Although the focus of these studies was depletion of filopodia, the cytochalasin treatment employed would have inhibited barbed-end actin polymerization generally.

The role of the Arp 2/3 complex in protrusive motility has also been subject to re-evaluation in non-neuronal cells. Several reports demonstrated that Arp depletion blocked lamellipodia and invadipodia formation (Harborth et al., 2001; Rogers et al., 2003; Yamaguchi et al., 2005), thus confirming the importance of Arp 2/3 in protrusion. However, other studies interfering with Arp function (Di Nardo et al., 2005; Gupton et al., 2005; Ng and Luo, 2004; Strasser et al., 2004) have reported continued motility, thus suggesting the existence of Arp2/3-independent mechanisms of protrusion. Finally, recent literature has identified actin nucleators other than Arp2/3 – namely, formins (Evangelista et al., 2003; Kovar, 2006; Zigmond, 2004) and spire proteins (Baum and Kunda, 2005; Quinlan et al., 2005; Schumacher et al., 2004), both of which nucleate linear actin filaments as opposed to branched ones. Such non-Arp nucleators taken together with the Arp depletion and perturbation experiments suggest that redundant pathways may exist for the protrusion of lamellipodia and veils. The alternative nucleation pathways also suggest that there is cell system dependent or conditional involvement of motility mechanisms.

Given the uncertainties surrounding the mechanisms that contribute to protrusive motility, we concluded that the presumed equivalence of neuronal growth cone veils and fibroblast lamellipodia required a closer evaluation. We felt that a kinetic-structural analysis of the growth cone veil similar to that which we carried out for keratocytes and fibroblasts (Svitkina and Borisy, 1999) was warranted. Examination of the growth cone literature indicated that no such study had yet been conducted. Most work that had addressed this topic occurred before current models of actin-based protrusive motility were available and before methodology was available to carry out correlative analysis at high resolution. The general conclusion that emerged was that an actin network existed in veils, often referred to as a 'cortical meshwork' (Clark et al., 1983; Landis, 1983; Lewis and Bridgman, 1992; Yamada et al., 1970; Yamada et al., 1971). These earlier studies, carried out at low resolution and lacking biomarkers such as Arp2/3 for the lamellipodium, were insufficient to answer questions regarding whether growth cone veils protruded by a similar or different mechanism from that of fibroblast or keratocyte lamellipodia.

Thus, a gap exists in our understanding of growth cone activity. We lack information on the supramolecular organization of the motility machinery in relationship to the dynamic behavior of protrusion and retraction. We have attempted to fill this gap by carrying out correlative light and electron microscopic analysis on chick dorsal root ganglion cells grown in explant culture. Time-lapse imaging of a living growth cone on a second-by-second time scale provided dynamics data on veil activity while platinum replica electron microscopy of the same veils allowed us to determine the supramolecular organization of the veils in a known state of behavior. The results obtained provide new information on the neuronal motility machinery and allow a conceptual framework to be formulated for understanding the structural basis of growth cone advance.

Results

Veils alternate phases of protrusion and retraction

Although many qualitative studies have characterized growth cone advance in terms of overall velocity and directionality, relatively few have provided detailed quantitative parameters. Bray and Chapman (Bray and Chapman, 1985) carried out a quantitative analysis of microspike movement but, as far as we are aware, the dynamics of veil movement have not been similarly deconstructed. In preparation for correlative electron microscopic analyses, we first determined basic parameters for growth cone behavior in our whole DRG explants. Confirming results in the literature (Argiro et al., 1984; Goldberg and Burmeister, 1986; Landis, 1983), growth cones of DRG axons advanced rapidly (1.09±0.34 μm/minute) with high persistence (0.9 over a period of 1 hour) for long periods of time (measured over 3-8 hours) (Fig. 1A). However, this relatively regular advance, evident from low-magnification, time-lapse images taken at intervals of minutes, belied the chaotic behavior evident at a time scale of seconds.

High magnification, high temporal resolution (2-3 seconds) image sequences showed significant shape changes in individual growth cones from frame to frame suggesting that the veils and filopodia that comprise the growth cone were changing on a rapid time scale. Kymographs were constructed for individual veils within growth cones to analyze their detailed behavior (Fig. 1B). As reported previously in qualitative terms (Goldberg and Burmeister, 1986; Tosney and Wessells, 1983), veils frequently showed periods of protrusion and retraction. Velocities of veil protrusion and retraction were obtained from the kymographs. Transitions between protrusion and retraction were defined by direction reversals observed in the kymograph. Durations of veil protrusion and retraction were calculated by dividing the total time protruding or retracting by the total number of transitions between protrusion and retraction.

The kymographs and quantitative data (Fig. 1C) indicated several aspects of veil behavior. First, veils alternated phases of protrusion and retraction with a small fraction of time spent in a paused or irregular state. The average duration of a protrusive phase at the front of the growth cone was about a minute, and transitions to retraction were abrupt. This indicates that for correlative electron microscopic analysis to capture characteristic features of a phase or a transition, it would need to be carried out with a temporal resolution of seconds.

Second, veil dynamics showed differences or similarities depending on position in the growth cone. Protrusion was somewhat faster (35%, P=0.016, two-tailed t-test) in the front compared with the rear of the growth cone, while retraction
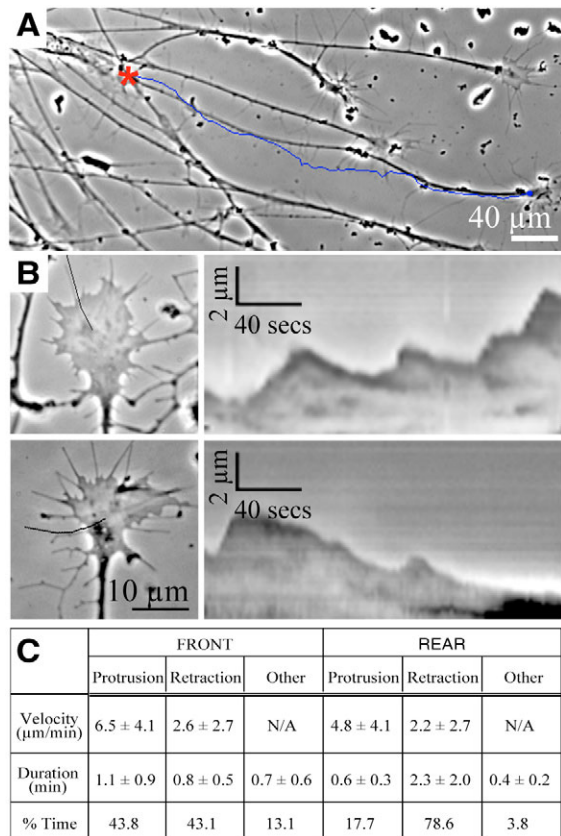
Fig. 1. Growth cone advance and veil dynamics. (A) Growth cone advance. Blue line traces path traveled by growth cone during a 3-hour time-lapse observation. * indicates start point. (B) Veil dynamics. Kymographs (right) of veils in growth cone front (top, left) and rear (bottom, left) show alternation of protrusion and retraction. Black line denotes path along which kymograph was obtained. (C) Orientation of protrusion and retraction phases. 'Other' denotes veil dynamics – collapse, ruffling or stalling – not readily categorized as protrusion or retraction. n=151 veils; 20 individual growth cones; 352 minutes observation; 329 transitions recorded.

Fig. 2. Veil protrusion and retraction are primarily filopodia associated. (A) Time-lapse merges illustrate veil categories. In this and all succeeding figures, protruding and retracting regions are indicated by red and cyan, respectively, by merging the later time point (red channel) with the earlier time point (blue and green channels). (a,b) Filopodia-associated protrusion – protrusion between two established filopodia. Veil edges can be convex (a) or concave (b). (c) Filopodia-independent protrusion – veil protrusion not connected to established filopodia. (d) Filopodia-associated retraction – retraction between two filopodia, retaining direct connection throughout retraction. (e, arrowhead) Filopodia-independent retraction is seen less than 3% of the time. (e, asterisk) Single filopodium-associated protrusion – protrusion along a single filopodium. (f, asterisk) Veil protrusion arising on a filopodium shaft. (B) Tabulation of frequency and width of veils in each category.

velocities did not vary significantly from the front to rear. However, at any given position along the growth cone perimeter, protrusion velocity was significantly greater (2.2× to 2.5×) than retraction velocity ($P<0.01$). In the front half of the growth cone, protrusion and retraction occurred for the same percentage of time and were similar in duration, whereas in the rear half of the growth cone, retraction occurred four times more frequently and lasted four times as long ($P<0.004$). Thus, the major differentiation between the front and rear of the growth cone was in the greater duration and frequency of retraction in the rear.

Third, veils protruded more rapidly (~6×) than the growth cone translocated: a property that requires explanation. Part of the explanation comes from the fact that individual veils protrude at various angles to the growth cone axis. For a veil protruding at an angle, ϕ, with respect to the direction of net advance, the contribution to the net velocity is the veil velocity times cos ϕ. Integrating over all orientations reduces average axial velocity by a half. The balance of the explanation comes from recognizing that retraction offsets much of protrusion.
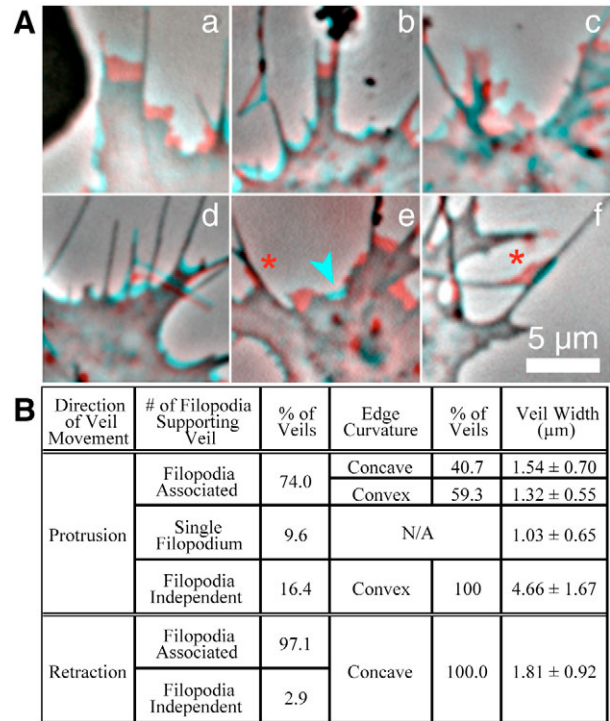
The overall rate of growth cone advance, v_{gc}, may be estimated from the parameters for individual veils as $=1/2 \, [v_p \, d_p \, f_p - v_r \, d_r \, f_r]$ where v, d and f are velocities, durations and fraction time in phase for protrusion (p) and retraction (r), respectively, in the front of the growth cone. Inserting the parameters from Fig. 1C gives v_{gc}=1.11 μm/minute, which corresponds surprisingly well to the measured rate of 1.09 μm/minute for overall growth cone advance. We conclude that growth cone advance may be accounted for on the basis of individual veil dynamics.

Veils can be categorized based on association with filopodia

Since growth cone behavior could be largely deconstructed into veil and filopodial behavior, we examined possible distinctions between veils as they related to filopodia. Veils were categorized as to whether they were protruding or retracting and whether they occurred between two adjacent filopodia, were associated with a single filopodium or were not associated with filopodia (Fig. 2A). Remarkably, 74% of protruding veils occurred between two filopodia less than 2.5
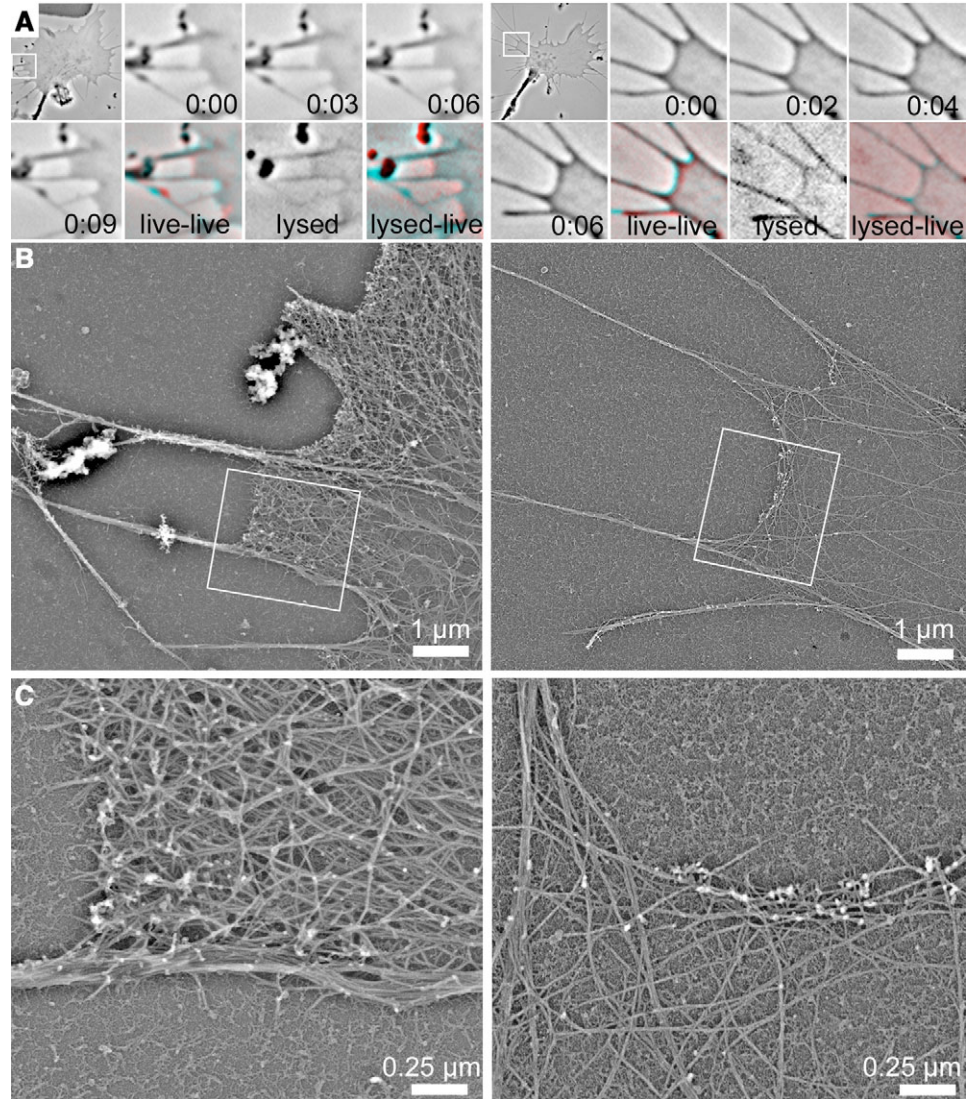
Fig. 3. Correlative light and electron microscopy of filopodia-associated veil protrusion and retraction. (A) Phase-contrast panels show a low magnification image of the growth cone with a white box denoting the region of interest, followed by four consecutive images from the last 9 seconds of the time-lapse sequence before the cell was extracted, a live-live phase-contrast merge of the first and last images, the same region after extraction 'lysed', and a phase-contrast merge of the lysed and the last live image. In all merges, red regions indicate protrusion, cyan regions indicate retraction. The veil in the left panel was protruding at 4.2 µm/minute, the veil in the right panel was retracting at 1.7 µm/minute. (B) Electron micrographs of region of interest from the time lapses in A. (C) Higher magnification of the boxed regions in B.

µm apart and an additional 10% occurred along a single filopodium (Fig. 2B). Often, veils would arise from the junction of two filopodia roots or in the 'crotch' of two filopodia diverging from a common trunk. Veil behavior seemed to occur in separable, independent units, frequently separated by a filopodium. The independent behavior of veils was manifested as protrusion on one side of a filopodium and retraction or pause on the other side. Thus, filopodia seemed to serve as 'boundaries' for veil formation. However, veils could often arise (16%) without obvious association with filopodia, which indicates that filopodia were not necessary for veil formation.

Veils were also categorized by shape because of the possibility that morphology would be indicative of mechanism. Lamellipodia of fibroblast-type cells typically display a convex shape because of protrusive forces pushing outward over a range of directions. Protruding veils not associated with filopodia also displayed a convex shape. However, veils associated with filopodia commonly displayed a concave shape. All retracting veils and approximately half of protruding veils were concave. A concave shape during retraction can be understood in terms of surface tension applied to the veil against filopodia that resist compression. However, the explanation for a concave shape during protrusion seemed counterintuitive; therefore, concave and convex protruding veils were subjected to separate analyses.

Correlative light and electron microscopy reveals structure-function relationships in veils

Correlative microscopy combines kinetic analysis of a living cell by light microscopy with structural analysis of the same cell by electron microscopy to determine the supramolecular organization of the cell in a known state of behavior (Svitkina and Borisy, 1998). For the growth cone, this means carrying out analyses on veils known to be protruding, retracting or in transition. As the most common form of both protruding and retracting veils was that associated with two filopodia, we first focused on this category (Fig. 3). The left panels of Fig. 3 show a protruding veil that had been protruding for ~21 seconds at the time of extraction and fixation. The 'live-live' panel is a color merge of the last two images of the living cell in which red indicates veil protrusion; cyan indicates retraction. The 'lysed-live' panel is a merge between the cell just after extraction and the last live image. A region of the growth cone
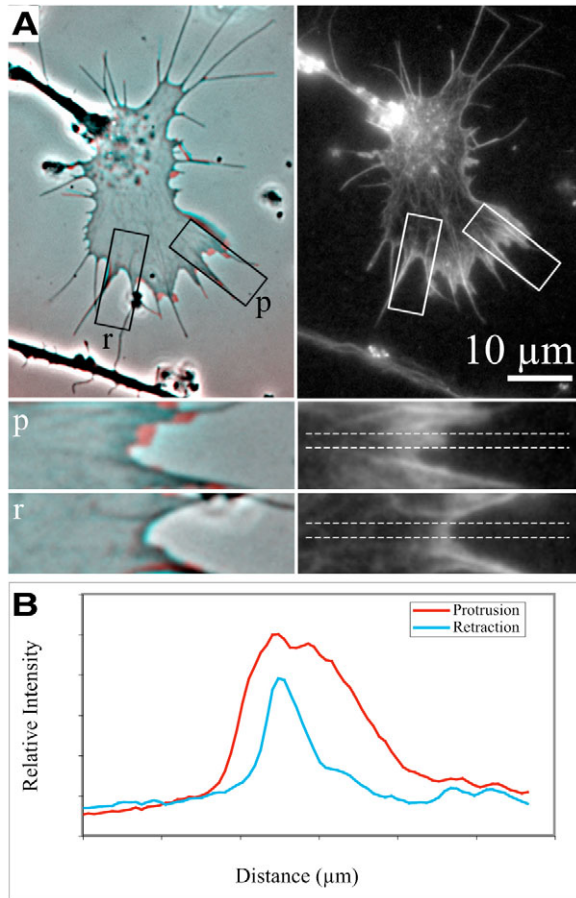
Fig. 4. Actin distribution in protruding and retracting veils. (A) Veil dynamics merge (left) and filamentous actin distribution (right) in a growth cone. The merge combines the last live phase-contrast image before extraction and the one obtained 6 seconds earlier. Enlarged insets (p, r) show regions of veil protrusion (red) and retraction (cyan). (B) Line scans of Texas Red phalloidin fluorescence for protrusion and retraction derived from the regions of the growth cone shown in A (dotted lines). Fluorescence was normalized to 100 at peak of protrusion distribution. Protruding veils have more and deeper filamentous actin than retracting veils. $n=4$ growth cones; 9 retracting veils; 22 protruding veils.

(white box) is shown in the low magnification electron micrograph (EM) and the veil under analysis is shown in the higher magnification EM. The protruding veil contains a dense, filamentous network that is bounded by the filopodia and comprised of both branched filaments and interspersed longer filaments. Overall, the appearance resembles that characteristic of fibroblast lamellipodia. At low magnification both associated filopodia can be clearly distinguished from the network. At high magnification, the network is in very close contact with the filopodia, and filaments appear to both enter into and/or come out of the filopodium.

The right panels of Fig. 3 show the kinetics and structure of three adjacent retracting veils that had been receding for almost 60 seconds at the time of extraction. They are strikingly different from protruding veils in ultrastructure, although the differences are not appreciable by phase-contrast microscopy. One difference is the density of filaments in the retracting veil.

Unlike the protruding veil, the filaments in retracting veils are scarce – sufficiently so that the background of the substrate is visible. A second difference is the organization of filaments. Filaments in retracting veils do not show a dendritic network; rather, they typically show filaments bundled and running parallel to the retracting edge.

The difference in filament density between protruding and retracting veils was sufficiently dramatic that we sought confirmation independent of processing for electron microscopy. We used fluorescently tagged phalloidin staining to quantify actin filament density (Svitkina et al., 1997) prior to preparation of the samples for electron microscopy. As shown in Fig. 4, linescan analysis of phalloidin staining indicated that protruding veils had a greater amount of actin (2$\times$) and a greater extent (depth) of the actin-rich region (3$\times$) than retracting veils. Additionally, we measured the total length of actin filaments contained in 0.25 μm^2 boxes drawn at the center of the edge of protruding and retracting veils. Protruding veils contained an average of 57.7±6.6 μm actin/μm^2, while retracting veils contained 19.8±4.0 μm actin/μm^2 ($n=10$ veils for each state, $P<0.00001$), which corresponds well with the phalloidin staining shown in Fig. 4. Thus, the disparity in filament density between protruding and retracting veils was not a consequence of sample preparation for electron microscopy.

A second line of evidence for the difference between protruding and retracting veils comes from analysis of phase transitions. Phase transitions are abrupt, occurring within one or two frames (3-6 s). For an average phase duration of approximately 60 seconds, this means that randomly picking the time of extraction and fixation for EMs will generate approximately 5-10% of the veils caught in a transition between retraction and protrusion. Such an event is illustrated in the left panel of Fig. 5. The cyan arrow in the live-live merged image shows a veil in a retraction phase, while the red arrow in the subsequent lysed-live image identifies a newly protruding veil that has formed in the same location during the time needed for lysis. The EMs show that the nascent veil is dense and dendritic in contrast to the sparse, unbranched network behind it. The structure of this transition suggests that the dendritic protruding veil appears to have formed by branching off the roots of the associated filopodia and/or the residual filaments of the previously retracting veil.

Finally, a third line of evidence comes from adjacent veils displaying opposite behavior. Adjacent veils that share a filopodium frequently exhibit independent behavior as illustrated in the right panels of Fig. 5. The lysed-live merge shows two adjacent veils (red and cyan arrows), separated by a single filopodium, that exhibit opposite behavior in which the lower veil protrudes and the upper veil retracts. The high magnification EM shows the sparseness of filamentous actin in the retracting veil adjacent to the robust dendritic network in the protruding veil. The correlation of filament density with veil behavior strongly suggests that the appearance of the network is not an artifact of processing for electron microscopy. Rather, the results indicate a significant difference in filament organization between protruding and retracting veils that has not been previously recognized.

Veils that protruded along single filopodia also showed a dense, dendritic network. In the nascent (4 seconds old) veil
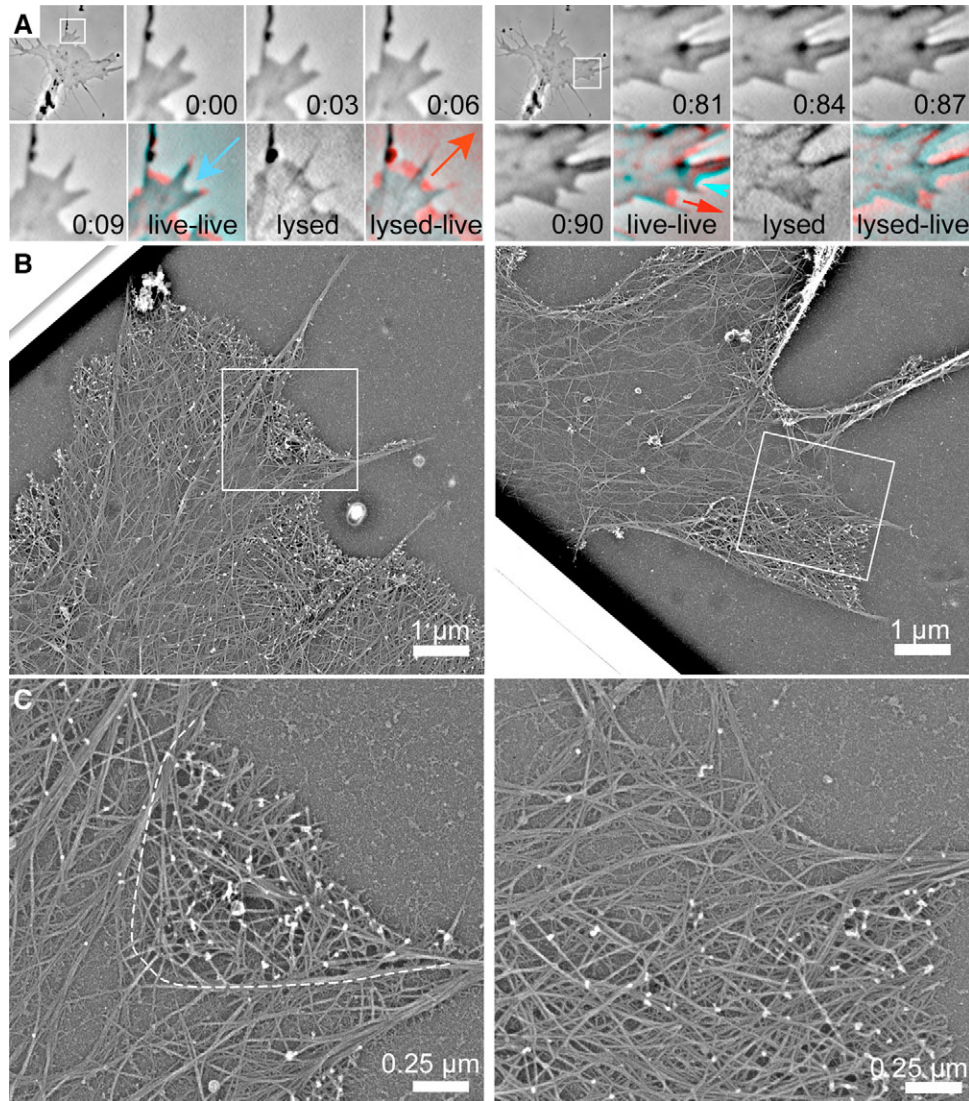
Fig. 5. Phase transitions and local autonomy of veils. Panel construction as in Fig. 4. (A) Left: nascent protrusion (3.6 μm/minute) characterized by dense branched network is demarcated from surrounding sparse network. Right: protruding (7.6 μm/minute) and retracting veil (2.8 μm/minute) adjacent to same filopodium show distinct filament organization: dense branched vs sparse, respectively. (B) Electron micrographs of the regions of interest from the time lapses in A. (C) Higher magnification of the boxed region in B. The new protrusion (left) is sharply demarcated from the local network (dashed line). Adjacent filopodia associated veils (right) have independent behavior.

shown in Fig. 6A, the surrounding region was retracting prior to the veil's appearance, while the filopodium was already present. Besides its dense network, the nascent veil contained long filaments that apparently connected to the filopodial shaft, while branches appear directed away from the shaft. Filopodia-associated veils can protrude in isolation from other veils and the body of the growth cone (Fig. 6B). In this example, the filaments in the associated filopodium merged near their base, isolating the veil from the rest of the growth cone. Filaments in the veil formed both branched and tightly bundled filaments. They are also seen growing out of and into the associated filopodia, which suggests that filaments can form by branching off from filopodia shafts. The average angle at which filaments branched off from filopodia was measured at 70.9±3.6° (n=51 branches, 8 growth cones).

Fig. 6C shows a typical filopodia-independent protrusion, whose network organization closely resembles the lamellipodia seen in fibroblasts and keratocytes (Svitkina and Borisy, 1999). The veil had been protruding for approximately 1 minute at the time of extraction, and contains a mixture of dense, branched network and embedded loosely bundled long filaments. Fig. 6D shows a group of nascent veils arising as multiple finger-like protrusions independent of any association with filopodia. These jutting protrusions are the usual precursor to the smooth-edged filopodia independent veil.

Taken together, the correlative microscopy experiments establish several new features of the growth cone motility machinery. The organization of actin filaments in protruding veils is similar to that in lamellipodia of fibroblasts: retracting veils lack a dendritic network but contain sparse long filaments, and dendritic networks can form from filopodia.
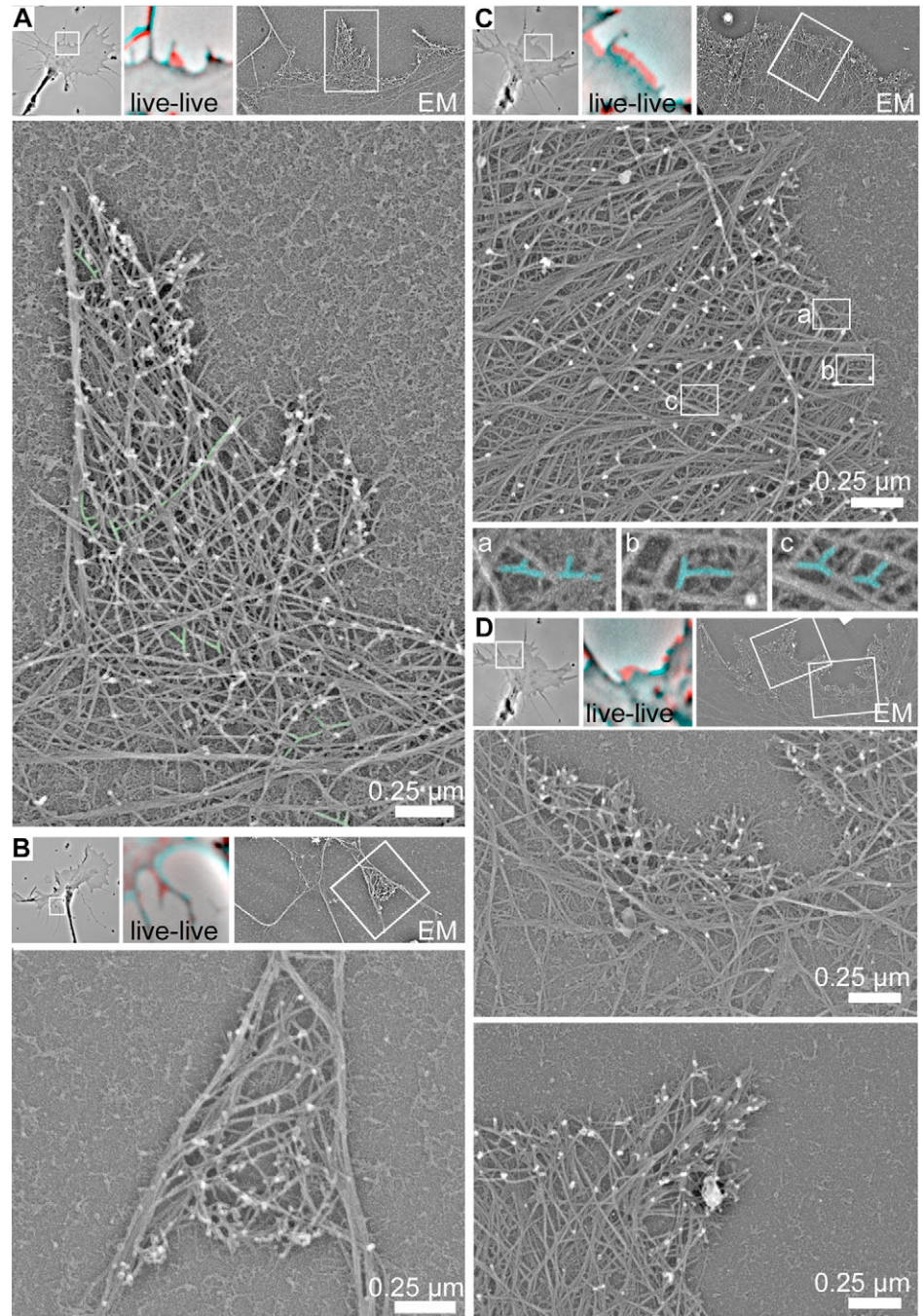
Fig. 6. Alternate forms of veil protrusion. The upper panel of each subsection contains a low magnification image of the growth cone, with the region of interest boxed, a single phase-contrast overlay, and a low magnification EM of the region of interest. (A) Nascent veil protrusion (6.8 μm/minute) along a single filopodium. Veil contains a dense network of filaments connected to filopodial shaft. (B) Veil formation (8.3 μm/minuts) isolated from lamellipodium. Dense network interconnects two filopodia shafts. (C) Established Filopodia 'independent' protrusion (8.1 μm/minute). Veil organization is a mixture of dense network and loosely bundled long filaments. Boxed regions (a-c) show branched filaments in the network, pseudo-colored cyan for visualization. (D) Nascent filopodia-'independent' protrusion (1.1 μm/minute). Veil displays multiple finger-like protrusions containing dense network and some long filaments.

Arp2/3 complex is localized to actin networks in veils and along filopodia

Since the supramolecular organization of filamentous actin in protruding veils appeared similar to that seen in the lamellipodia of motile fibroblasts and keratocytes, we tested whether veils contained the Arp2/3 complex, a biomarker characteristic of dendritic networks. Fluorescence immunostaining for Arp3 demonstrated, at the light microscopic level, that Arp3 was enriched at the leading edge of the growth cone and co-localized with phalloidin-stained actin filaments (Fig. 7A). We also stained for the p34 subunit, using an alternative fixation technique, and saw similar staining patterns in both DRG and PC-12 growth cones

(supplementary material Fig. S1A-C). Control staining and immunoblotting demonstrated specificity of both antibodies (supplementary material Fig. S2A-C). Expression of myc-tagged Arp3 in NG108 cells as evaluated by immunostaining (supplementary material Fig. S2D) and expression of GFP-tagged Arp3 in PC-12 growth cones as evaluated by TIRF (total internal reflection fluorescence) microscopy showed localization of the expressed protein at the leading edge of protruding growth cone veils (supplementary material Fig. S3). Thus, on the basis of immunostaining and expression data, the Arp2/3 complex seemed to be present in the growth cone.

To localize the Arp2/3 complex at higher resolution and to evaluate Arp localization in relation to its protrusion history,
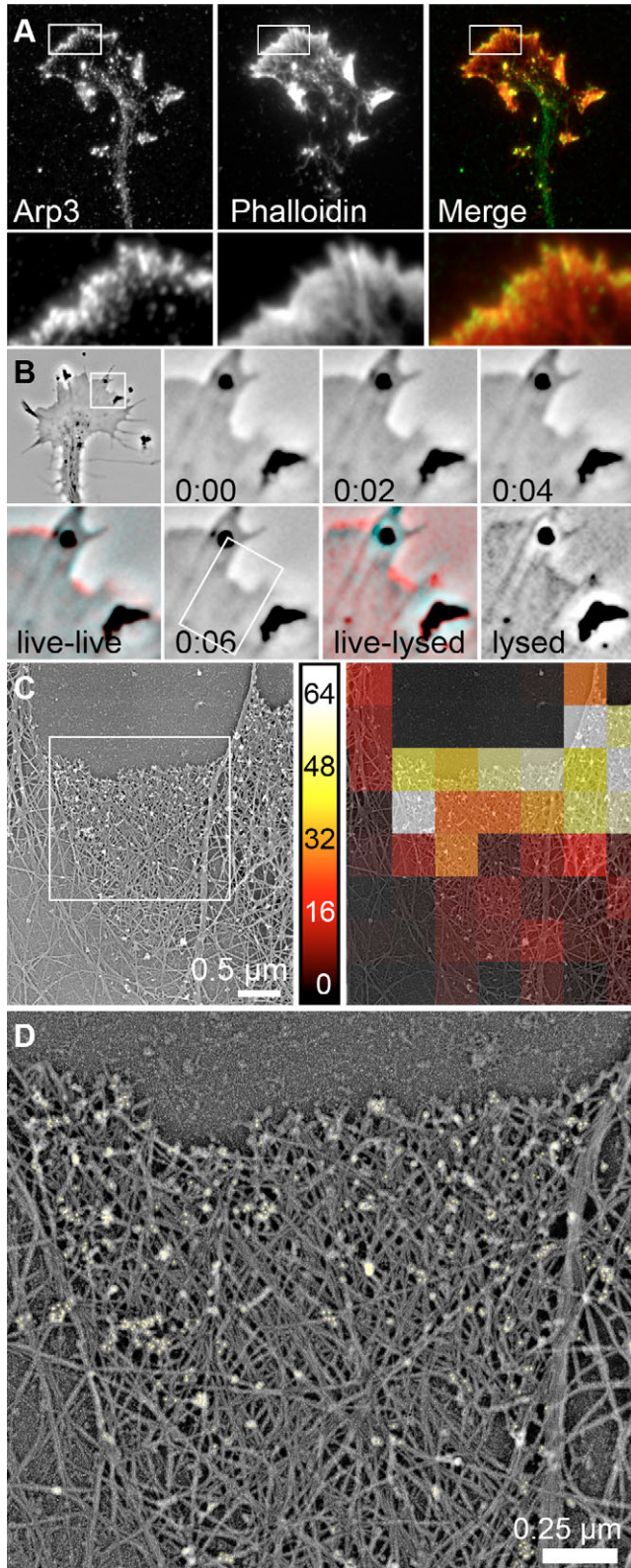
Fig. 7. Distribution of Arp2/3 in veils. (A) Growth cone immunostained against Arp3 subunit and phalloidin. Inset shows an enrichment of Arp3 (green) at the leading edge that co-localizes with phalloidin stained actin (red). (B) Low magnification growth cone (veil protrusion at 5.3 μm/minute) followed by time lapse and merges of boxed region. (C) Left. EM of region in lysed-live in B immunostained against Arp3 subunit. Right. Same EM overlaid with a 0.5 μm grid colored to reflect the number of gold particles in each box; heat map indicates number of gold particles per 0.25 μm^2 box. Similar to A, Arp3 staining co-localizes with actin and is highest at the leading edge of protruding veils. (D) High magnification of the boxed region from C. Gold particles have been pseudo-colored yellow.

fill a box, the count was normalized to the area of a 0.5 μm box). The 'heat map' reflecting the number of gold particles (Fig. 7C, right) indicates that the Arp2/3 complex was highest in concentration at the leading edge of the protruding veils and was localized to the dense dendritic network (as opposed to regions with bundles of long filaments). Protruding veils contained an average of 145±20 gold particles per μm^2 at the leading edge, and 60±9 gold particles per μm^2 that were 1 μm away from the leading edge, while retracting veils contained only 17±7 gold particles per μm^2 at the retracting edge, and 11±6 gold particles per μm^2 that were 1 μm away from the retracting edge (*n*=8 protruding and 8 retracting veils). In less dense regions of protruding veils, gold particles were localized to individual Y junctions (supplementary material Fig. S4). Sparse non-protruding regions were not enriched in gold particles. Control growth cones stained only with secondary antibody labeled with gold particles contained very few gold particles (supplementary material Fig. S2E). Inset shows Arp3 staining (Fig. 7D) with gold particles pseudo-colored yellow for easier visualization.

Veils sometimes protruded with a concave shaped leading edge. Because such a shape is characteristic of retracting veils, we wondered whether concave protrusions proceeded by a different mechanism from that of convex protrusions and so tested whether Arp2/3 was present in such veils. We found that Arp2/3 in concave veil edges varied with direction of veil movement. Arp2/3 was found in veils protruding with a concave leading edge (Fig. 8A) but was not enriched in retracting veils (Fig. 8B). In this figure, the veil had been retracting for ~40 seconds, displaying the usual concave edge. Typical of retracting veils, there was little underlying network. The network that did remain was not enriched with Arp2/3.

Arp2/3 was also found in veils that spontaneously formed along the shafts of filopodia. Fig. 8C shows a small veil (*) that formed at the distal end of a filopodium, and then traveled down the filopodium shaft. The live-live merge and the low magnification EMs show the veil as it approached the second filopodium and then began to protrude between the two filopodia. The network contains loosely bundled long filaments mixed with a dense branched network that stained for Arp3. Fig. 8D shows a small veil that formed at a kink along the shaft of a filopodium over ~6 seconds. By light microscopy it appeared as a dark expanding spot along the shaft of the filopodium. Electron microscopy showed that the nascent veil contained a dendritic network enriched with Arp2/3 that was associated directly with filaments of the filopodium shaft.

immunogold electron microscopic staining was carried out using correlative microscopy (Fig. 7B-D). The EM of the protruding veil in the lysed-live merge (Fig. 7C, left) was overlayed with a 0.5 μm grid, and the number of 10 nm gold particles in each box was counted (for veil regions that did not

Thus, nascent veils that form along the length of filopodia are dendritic and associated with Arp2/3 just as veils that form between filopodia.

Discussion

The main goal of this study was to elucidate the organization of the actin cytoskeleton underlying veil movements. Our results provide a significant advance in three respects: first, we show that protruding veils are comprised of a densely branched network of actin filaments that is lamellipodial in appearance and includes the Arp2/3 complex. On the basis of this structural and biomarker evidence, we infer that the dendritic nucleation/array-treadmilling mechanism of protrusive motility (Pollard and Borisy, 2003) is conserved in the veil protrusion of growth cone advance as in the motility of fibroblasts and keratocytes. Second, we delineate the supramolecular organization of the retraction phase, a phase originally reported by Abercrombie (Abercrombie et al., 1970; Abercrombie et al., 1971) in the crawling movement of fibroblasts but which has not previously been specifically analyzed at a high resolution structural level. Veil retraction, in contrast to protrusion, was characterized by sparse, long filaments, some of which are bundled parallel to the cell edge. Third, we show that filopodia have the capacity to nucleate dendritic networks along their length, a property consistent with veil formation seen at the light microscopic level but not previously understood in supramolecular terms. The basic findings of this study are summarized in Fig. 9. We discuss each of these findings in turn and then comment on how they can be viewed as elements of motility which, when taken together, provide a conceptual framework for understanding the structural basis of growth cone advance.

Veil protrusion

Correlative light and electron microscopy permits a kinetic-structural analysis of a cellular process. Temporal resolution of the kinetics is determined by the interval of time-lapse imaging and the time required for lysis and fixation (~3 seconds). Spatial resolution is limited by the grain of the platinum (~3 nm) in the replica approach. Analysis of veils undergoing a transition from retraction to protrusion indicated that formation
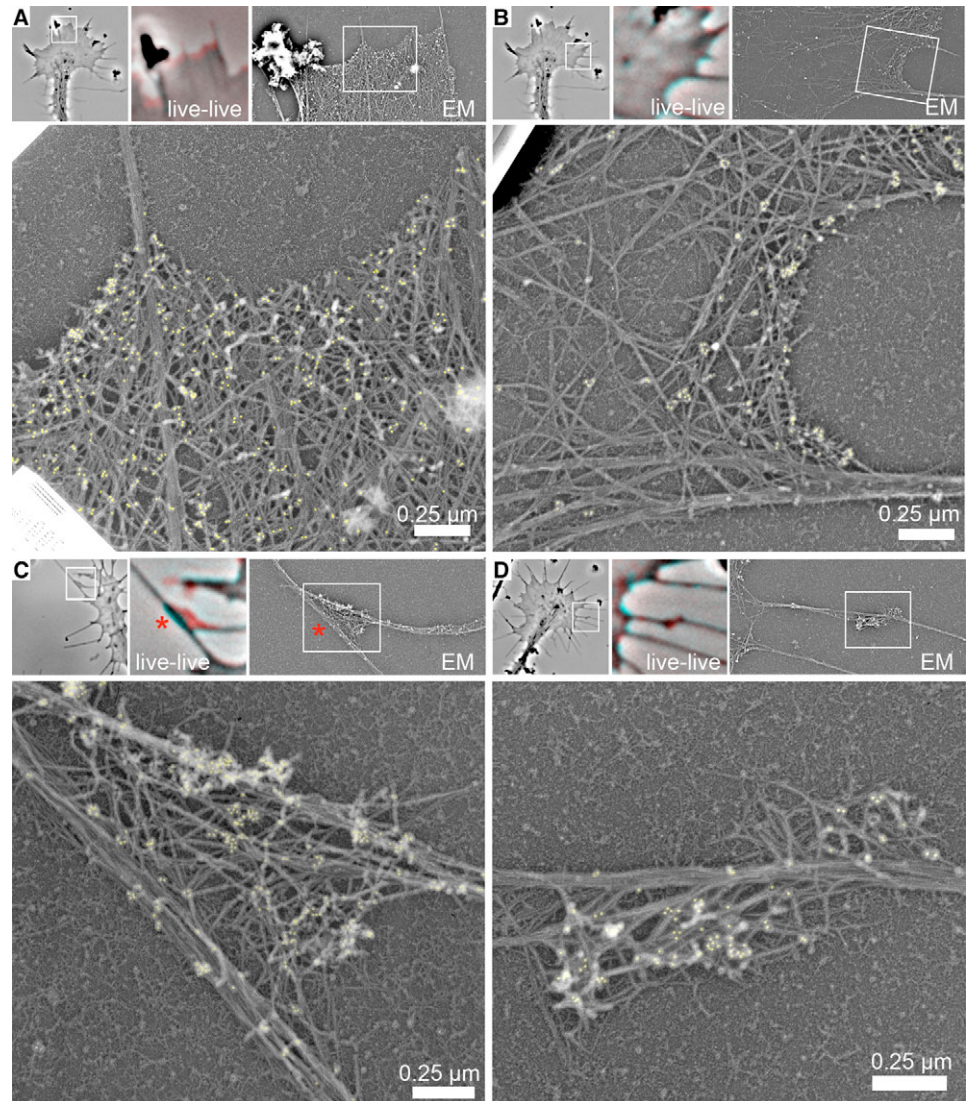

Fig. 8. Correlation of Arp3 location with veil dynamics. The upper panel of each subsection contains a low magnification image of the growth cone, with the region of interest boxed, a single phase-contrast overlay, and a low magnification EM immunostained against Arp3 in the region of interest. (A) Protruding filopodia (5.2 μm/minute)-associated veil with a concave leading edge. (B) Retracting filopodia (1.7 μm/minute)-associated veil with sparse actin network. (C) De novo veil initiation from filopodial shaft (*), which travels (11.3 μm/minute) toward the growth cone. (D) Representative example of a veil arising de novo from a phase-dense spot along the shaft of a filopodium.

of a branched, lamellipodia-like network was rapid, occurring within seconds after the phase transition. At veil protrusion velocities of 6 μm/minute, electron microscopy established that about 1 μm of nascent dendritic network could be formed within approximately 10 seconds. This is consistent with rates of actin polymerization and lamellipodial formation in fibroblasts.

The conclusion that veil protrusion is dendritic in nature is not simply a confirmatory finding for neurons of a mechanism accepted in fibroblasts. Strasser et al. found that Arp was paradoxically enriched in the central domains of the growth cone and neurites rather than in the veils, and that the ultrastructure appeared to contain few Y junctions, raising the
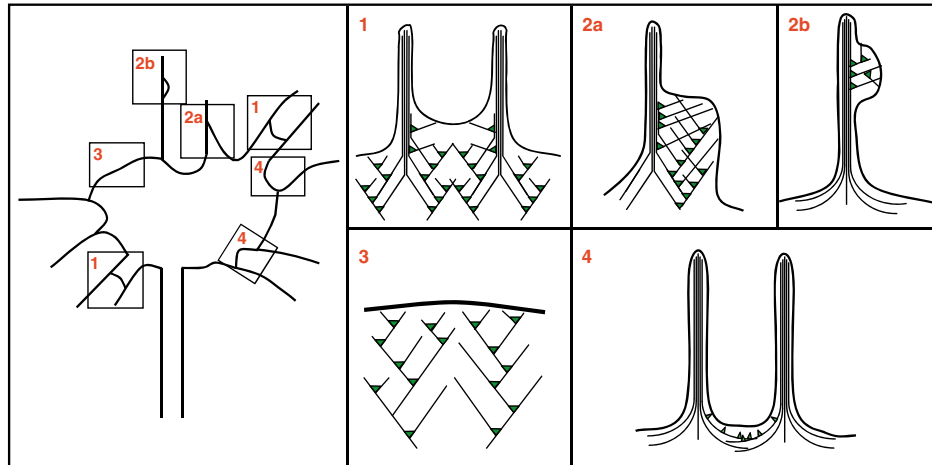
Fig. 9. Modes of veil dynamics in the neuronal growth cone. (1) Veil protrusion associated with filopodia at the front and rear of the growth cone. Branched filaments can arise from the veil network and merge into the filopodia or can occur off existing filaments in the filopodia. (2) Veil protrusion along a single filopodium, either crawling along the side of the filopodium (2a) or arising de novo off the shaft of the filopodium (2b). (3) Veil protrusion independent of filopodia. The veil network appears to be similar to lamellipodial network seen in non-neuronal cells. (4) Retraction at the front and rear of the growth cone. The veil network becomes very sparse and some filaments are seen aligned and bundled, parallel to the membrane.

question of what type of cytoskeletal organization was present in protruding veils (Strasser et al., 2004). Additionally, as outlined in the Introduction, recent studies involving mutation (Ng and Luo, 2004) or expression of a dominant negative construct (Strasser et al., 2004) have called into question whether neuronal advance proceeds by an Arp2/3-dependent mechanism. In both studies, although axon outgrowth occurred, pathfinding was aberrant. Our kinetic-structural results establish that the dendritic pathway does function in DRG growth cones that protrude veils under normal culture conditions. Further, the dendritic pathway biomarker, Arp2/3, was localized to the leading edge of protruding veils by both immunostaining and by expression of tagged Arp2/3 (both Myc and GFP). It is not clear why this staining pattern was not seen in the study of Strasser et al. (Strasser et al., 2004), but one possibility is that their wide field imaging missed the edge localization because of the greatly differing optical thickness of the neuronal shaft versus the lamellipodium [see Grzywa et al. (Grzywa et al., 2006) and comparison of TIRF and widefield imaging of growth cones in supplementary material Fig. S3A]. Alternatively, it is possible that the observed aberrant pathfinding reported in Arp2/3-deficient neurons (Ng and Luo, 2004; Strasser et al., 2004) indicates that Arp2/3-mediated dendritic nucleation may be critical for the exploratory functions of growth cones, required for pathfinding, while expendable for neurite extension.

Further, the role of the Arp 2/3 complex in protrusive motility has been subject to re-evaluation in non-neuronal cells with results both supporting (Harborth et al., 2001; Rogers et al., 2003; Yamaguchi et al., 2005) and in opposition (Di Nardo et al., 2005; Gupton et al., 2005; Ng and Luo, 2004; Strasser et al., 2004) to an essential role for Arp2/3. Such mixed results in the literature suggest that there is a cell system specific or conditional involvement by motility mechanisms. Moreover, redundant pathways probably exist for the protrusion of lamellipodia and veils. Unraveling the relative contribution of

the pathways will require quantitative analyses in which each pathway is individually perturbed.

Veil retraction

Although fibroblast motility was originally described in terms of alternating phases of protrusion and retraction (Abercrombie et al., 1970; Abercrombie et al., 1971), the protrusion phase has received most attention while the retraction phase has been relatively understudied. To our knowledge, no detailed kinetic-structural studies at the supramolecular level have been carried out on retraction in any cell system. One reason for this may be that in non-neuronal cells the lamellipodium overlaps spatially with the lamellum (Gupton et al., 2005), thus obscuring clear views of the lamellipodium in retraction.

In the growth cone, in contrast to fibroblasts, the motility machinery is separated from the remainder of the organelles and nucleus in the cell body. Growth cones microsurgically severed from the cell body have the capacity to continue to move (Bray et al., 1978). Thus, the motility machinery of the growth cone, to a first approximation, is autonomous. The spatial separation and local autonomy of the growth cone may provide unique advantages for studying the motility machinery in general and retraction in particular.

Previous studies have characterized the growth cone in terms of peripheral, actin-rich, and central, microtubule-rich domains with a transitional domain defining the boundary between them (Bridgman and Dailey, 1989; Forscher and Smith, 1988; Smith, 1988). Veils are considered to be in the actin-rich, peripheral domain. However, previous studies have not attempted to seek distinctions in structure between protruding and retracting veils.

Our results showed that retracting veils, in contrast to protruding veils, contain a sparse array of long actin filaments and that some of these filaments tend to run parallel to the retracting cell perimeter and are organized into bundles. Typically, the retracting edge was concave and the actin

bundles paralleled this edge. Analysis of the transition from the protrusion phase to the retraction phase indicated that the dense, dendritic network of the protrusion phase was lost rapidly (within tens of seconds) after the retraction phase began. The kinetics of this loss are consistent with an array treadmilling mechanism (Pollard and Borisy, 2003) in which polymerization at the barbed end of actin filaments near the membrane is turned off; continued depolymerization at the pointed end would then result in disappearance of the dense, branched network and represent the initial phase of veil retraction. The remaining, long filaments presumably provide mechanical connection between the retracting edge and the deeper cytoplasm. Edges that continue to retract continue to show the sparse array of long filaments. Although this mode of organization may be unique to retracting veils of neuronal growth cones, it also seems possible that this is a general pattern of organization that is present in fibroblasts and other motile cells but which is simply more clearly visualized in neurons.

The mechanism responsible for formation of the parallel bundled filaments underlying the membrane in veil retraction has not been investigated but may be related to the edge actin bundles originally described by Albrecht-Buehler (Zand and Albrecht-Buehler, 1989), or it may be related to the phenomenon of retrograde flow and to forces generated by myosin II. Once actin polymerization is blocked at the leading edge, the actin filament network rapidly flows backwards with retrograde flow; inhibition of myosin II in neurons blocks retrograde flow in the transitional domain, and leads to a 50% decrease in retrograde flow in the peripheral domain (Medeiros et al., 2006). Myosin II has been immunolocalized to the central and transitional regions of the growth cone, and has also been localized at the edge of retracting veils (Rochlin et al., 1995). Further, myosin II has been correlated with formation of parallel bundles at the rear of the dendritic network in keratocytes (Svitkina et al., 1997). Taken together, these results point to an important role for myosin II in continued veil retraction. Our electron microscopy results show that the actin network, a few microns behind the protruding edge, is already quite sparse. The combination of a sparse network, rapid retrograde flow, and myosin-driven bundling could provide an explanation for the observed supramolecular organization found in retracting veils of growth cones.

Veil formation on filopodia

Our results suggest that filopodia demarcate boundaries between veils and have the capacity to initiate the formation of nascent veils. Our light microscopic observations revealed that most veils were associated with at least one filopodium, which were consistent with the literature (Goldberg and Burmeister, 1986), whereas the ability of adjacent veils to behave independently while sharing a single filopodium was a novel result. Frequently, veils were observed protruding on one side of a filopodium while retracting on the other side. In such cases, electron microscopy revealed a dramatically different mode of actin organization on either side of the filopodium – dense, branched network on the protruding side and sparse network on the retracting side. Filaments from one veil did not appear to extend over the shaft to interact with filaments of the adjacent veil. Thus, the supramolecular organization seen in these veils supports the idea of locally independent units of veil behavior.

Beyond demarcating boundaries between veils, filopodia appear to play an active role in veil formation. Routinely, we observed in phase-contrast time-lapse sequences that veils would be initiated along filopodial shafts or in the 'crotch' of forked filopodia, far from the growth cone or nearby veils. In all cases evaluated by correlative electron microscopy, the veil was revealed to contain a dense, branched actin network, enriched in Arp2/3 and associated with the filaments in the filopodium. Filaments in the veil were frequently seen branching off filaments in the filopodial shaft at an angle suggestive of Arp2/3 nucleation. This result was initially surprising since Arp2/3 was not previously thought to be present in filopodia, though at least one of its activators had been localized there (Nozumi et al., 2003). Our results carry implications for veil formation and current models for lamellipodial formation as well.

Nucleation of actin filaments from filopodial filaments presumably represents nucleation on the side of actin filaments. Although actin filaments have been demonstrated to support side branching in vitro (Higgs and Pollard, 1999; Higgs and Pollard, 2001; Mullins et al., 1998), the typical situation in vivo restricts branching to sites near the barbed ends of actin filaments in close proximity to the cell membrane because that is where activators of Arp2/3 are located (Pantaloni et al., 2000; Pantaloni et al., 2001; Wiesner et al., 2003). The appearance of actin filaments branching from the sides of filopodia has not previously been reported in vivo. Filaments in filopodia are thought to be long and have their barbed ends near the filopodial tip. Veil formation along the length of filopodia, therefore, may be a realization of the capacity of actin filaments to support side branching. From these results we can expand upon the convergent elongation model for filopodia formation (Svitkina et al., 2003) that accounts for the emergence of bundled filaments from the dendritic network. Our data add to this model the possible re-emergence of a branched network from filopodia – allowing the filopodia to continue to interact with both the network from which it formed and the new one which it initiates.

An additional caveat is that veil formation off the side of filopodia could potentially influence the shape of the leading edge of the veil. Veil initiation along a filopodium shaft would begin protruding distal to the leading edge of the connected veil, creating the observed concave protruding edge. It has been reported that adhesions along the filopodial shaft regulate veil advance along filopodia, and this could be a possible mechanism by which this occurs (Steketee and Tosney, 2002). Taken together, veil protrusion and veil formation on filopodia allow the creation of great diversity of form, from a very basic organization of the actin cytoskeleton (Fig. 9).

In summary, our results suggest that the plasticity of growth cone motility arises at the level of individual veils associated with filopodia within the growth cone. Individual veils exhibit directional instability, alternating between rapid phases of protrusion and retraction. This property allows for focal response to the encountered environment. Since the growth cone is composed of an ensemble of protruding and retracting veils, net growth cone advance may be considered the vector sum of all veils' motility behavior in response to their local environments. Filopodia play a key role in delimiting veils and serving to nucleate the formation of new veils. In the case of the path-finding growth cone, this system is particularly

economical. It allows exploration of the environment by numerous long filopodia, selective protrusion along the filopodia that find a good path, and rapid disassembly of veils that protruded along a non-productive path.

Materials and Methods

Cell culture
Whole chicken dorsal root ganglion neurons (DRGs) were isolated from E7-E9 chick embryos as described (Smith, 1998). Briefly, whole DRG explants were cultured in D-MEM/F-12 (Invitrogen; 11039-021) with 15 mM HEPES buffer, L-glutamine, and pyridoxine HCl; without Phenol Red and pyridoxal HCl base media supplemented with: 1 mg/ml bovine serum albumin fraction V powder (Sigma; A-9647), 5 μg/ml crystalline bovine pancreas insulin (Sigma; I-6634), 0.025 μl sodium selenite (Sigma; S-9133), 10 μg/ml chick transferrin (Intercell Technology; F-811), and 5-10 ng/ml 7s-NGF (Sigma). DRG explants were plated on ethanol-cleaned glass coverslips or glass bottom imaging dishes coated with 0.01% (w/v) poly-D/L-ornithine or poly-D-Lysine solution overnight (Sigma; P-4597 or P4707). Rat pheochromocytoma cells (PC-12) cells were obtained from ATCC (ATCC CRL-1721) and were cultured in Dulbecco's modified Eagle medium (DMEM) supplemented with 10% horse serum (HS), 5% fetal bovine serum (FBS), 1:100 penicillin/streptomycin, 1:100 sodium pyruvate. Process extension was elicited by transferring cells into DMEM supplemented with 5% FBS and 50-100 ng/ml 2.5S mouse NGF. Mouse/rat neuroblastoma cells (NG108) cells were cultured in DMEM supplemented with 10% fetal bovine serum (FBS), 1:100 penicillin/streptomycin, and 1× HAT (hypoxanthine).

Light microscopy
Light and fluorescence microscopy were performed using an inverted microscope (Diaphot 300; Nikon) equipped with Plan, 63× objective, and (TMD) 10× objectives and a back-illuminated, cooled CCD camera (model CH250, Roper Scientific) or a slow-scan cooled CCD camera (model CH350, Photometrics) driven by MetaMorph Imaging software (Universal Imaging). For live cell imaging, cells were kept at 36-37°C by means of an objective heating system. For overnight imaging, the media in culture dishes was overlayered with mineral oil to reduce evaporation. Filter cubes and filter wheel sets were used for fluorescence imaging.

Growth cone tracking, kymography, and linescan analyses
Low magnification (10×, phase-contrast objective) time-lapse movies were made to track axonal outgrowth. Images were acquired every 3 minutes over 3-8 hours. Growth cone translocation tracks were obtained by recording the location of the center of the growth cone in each frame of the image sequence using NIH Image J software (Abramoff et al., 2004). Instantaneous velocities were calculated from differences in growth cone position in successive frames. Persistence of translocation over a 1 hour period was calculated as the ratio of the straight line distance between start and end points and the actual path distance obtained by summing the distances between every pair of successive frames.

For kymography, phase-contrast time-lapse sequences were obtained on a Nikon Diaphot 300 microscope using a 63× objective. Movies were 2 minutes to 8 hours long with frames taken every 2-3 seconds for shorter movies and every 3 minutes for sequences longer than 15 minutes. Kymographs were produced using the NIH ImageJ software 'kymograph' function after the image sequence was first processed with the 'enhance contrast' function to maximize the contrast of the veil edge against the background (Abramoff et al., 2004). A 1-pixel-wide path was drawn perpendicular to the direction of veil protrusion or retraction (x-axis, measured in μm). Time is measured along the y-axis in seconds, with 2-3 seconds between each line depending on acquisition rate of the specific timelapse. Slopes of these lines were used to calculate the velocities, and projections of these lines along the x-axis (time) were used to calculate the duration of protrusions essentially as described (Hinz et al., 1999). The direction of veil protrusion was represented in text figures by color merging successive frames, either by merging two live frames or by merging the lysed and last live frames of the image sequence. In all cases, the later image was put in the red channel and the earlier image in the blue and green channels. Merging the images thus resulted in color-coding of protruding domains as red and retracting domains as cyan.

Linescan analyses of actin intensity were performed using the NIH ImageJ software, 'plot profile' function, using a 3-7-pixel-wide line on phalloidin-stained growth cones. Values were normalized to obtain relative intensities.

Immunofluorescent staining of fixed cells
Before staining with Arp3, cells were extracted to expose the cytoskeleton and corresponding epitopes and then fixed. Extraction with a non-ionic detergent (1% Triton-X) was used to solubilize rapidly the cell membrane, and stabilizers such as phalloidin (to stabilize actin specifically) and high molecular weight polyethyleneglycol (PEG) in PEM buffer were used to prevent redistribution of components during sample preparation. Briefly, culture media was removed from the dish and cells were rinsed with PBS to remove serum. Cells were extracted by incubation for 3-5 minutes at room temperature in extraction buffer (contains: 1% Triton-X, 4% PEG M_r 40,000 (SERVA), 10 μM phalloidin, and 10 μm taxol in PEM buffer) and then rinsed twice in PBS for 5 minutes. Extraction was followed by glutaraldehyde fixation: 0.2% glutaraldehyde made in 0.1 M cacodylic acetate, and quenched twice in 2 mg/ml sodium borohydride for 10 minutes to reduce background auto-fluorescence. Cells immunostained against p34 were fixed directly in 4% paraformaldehyde in PBS for 5 minutes, permeabilized in 1% Triton-X 100 in PBS for 3 minutes, and rinsed three times in PBS before application of primary antibody. Anti-Arp3 (1:35) and anti-p34 (1:50) (Upstate Biotech) primary antibodies were used to detect Arp2/3. All secondary antibodies for immunofluorescence were obtained from Jackson Laboratories or Sigma.

Correlative light and electron microscopy (with or without immunoelectron staining)
Samples for platinum replica electron microscopy were prepared as described in Svitkina and Borisy (Svitkina and Borisy, 1998). Briefly, whole DRG explants were plated onto gold, poly-D-Lysine, and laminin coated grid-finder coverslips attached via vacuum grease to plastic imaging dishes with a hole bored in the bottom. Explants were allowed to grow for ~24 hours before imaging with a 60X heated objective on a Nikon Diaphot 300 microscope with motorized stage. Phase-contrast images of the selected growth cone(s) were acquired every 2-3 seconds for 30 seconds to 3 minutes, until the growth cone appeared in a stable state of well attached protrusion. Culture media was vacuum aspirated and extraction solution (1% Triton X-100, 4% PEG (MW 40,000) (Serva, Heidelberg / New York)) in buffer PEM supplemented with 10 μg/ml taxol and 10 μM phalloidin) was immediately added while imaging continued. Phase-contrast images were obscured for approximately 4-6 seconds during this process. Extraction solution was aspirated after 4 minutes, the dish was rinsed 2X in buffer PEM, and then the sample was incubated with 2% glutaraldehyde in 0.1M cacodylic acid for 20 minutes to fix the cytoskeleton.

At this point, some samples were stained for filamentous actin by a 10-minute incubation with 1:100-200 dilution of fluorescently labeled phalloidin in PBS. To prevent photodamage to the cytoskeleton prior to visualization in the EM, fluorescent imaging was minimized – generally no more than 2-3 fluorescent images were acquired with short exposure time (~100 mseconds). Samples were prepared for immunoEM localization of biomarkers as follows: fixed cytoskeletal preparations were quenched by applying 2 mg/ml sodium borohydride (NaBH4) in PBS (2×, 10 minutes each) at room temperature. Dishes were rinsed in PBS (3×, 5 minutes), PBS was removed, and coverslips were wiped around the central finder grid to allow primary antibody application in PBS (Arp3, 1:10), and incubated 30-45 minutes at room temperature. After rinsing in PBS (3×, 5 minutes), coverslips were rinsed once with buffer A (20 mM Tris-HCl, pH 8.0, 0.5 M NaCl, 0.05% Tween 20) containing 0.1% BSA, and coverslips were again wiped around the central finder grid before applying secondary gold-conjugated antibody in Buffer A with 1.0% BSA, overnight at room temperature in a moist sealed dish. Dishes were rinsed in buffer A containing 0.1% BSA (3×, 5 minutes) and fixed again in 2% glutaraldehyde in 0.1 M cacodylic acid for 20 minutes.

Without washing, glutaraldehyde was removed, 0.1% tannic acid solution was added (Mallinckrodt, Paris, Kentucky; Cat. no. 1764) and dishes were incubated for 20 minutes at room temperature. Specimens were rinsed in water (3×, 5 minutes). 0.1-0.2% aqueous uranyl acetate solution was added and samples were incubated for 20 minutes at room temperature. Dishes were rinsed with distilled water and then samples were dehydrated through 5 minute incubations in graded ethanols (10%, 20%, 40%, 60%, 80%, and twice in 100%). Dishes were incubated in 0.1-0.2% uranyl acetate in 100% ethanol for 20 minutes, then washed twice in 100% ethanol and twice in 100% ethanol dried over molecular sieves, 5 minutes in each. Samples were placed in the critical point dryer and ethanol was substituted with liquid CO_2 at 5-10°C by 10 exchanges for 5 minutes each. Samples were then placed in a vacuum evaporator and shadowed with 2-2.8 nm platinum, followed by carbon evaporation coating of 2-3 nm. Individual samples were located under the microscope and mounted on EM grids for observation.

Statistics
Significance was determined using a two-tailed Student's t-test, P values are given in the text; P values less than 0.05 were considered significant.

References
Abercrombie, M., Heaysman, J. E. and Pegrum, S. M. (1970). The locomotion of fibroblasts in culture. II. 'RRuffling'. *Exp. Cell Res.* **60**, 437-444.
Abercrombie, M., Heaysman, J. E. and Pegrum, S. M. (1971). The locomotion of

fibroblasts in culture. IV. Electron microscopy of the leading lamella. *Exp. Cell Res.* **67**, 359-367.

Abramoff, M. D., Magelhaes, P. J. and Ram, S. J. (2004). Image processing with ImageJ. *Biophotonics Int.* **11**, 36-42.

Argiro, V., Bunge, M. B. and Johnson, M. I. (1984). Correlation between growth form and movement and their dependence on neuronal age. *J. Neurosci.* **4**, 3051-3062.

Baum, B. and Kunda, P. (2005). Actin nucleation: spire–actin nucleator in a class of its own. *Curr. Biol.* **15**, R305-R308.

Bentley, D. and Toroian-Raymond, A. (1986). Disoriented pathfinding by pioneer neurone growth cones deprived of filopodia by cytochalasin treatment. *Nature* **323**, 712-715.

Bernheim-Groswasser, A., Wiesner, S., Golsteyn, R. M., Carlier, M. F. and Sykes, C. (2002). The dynamics of actin-based motility depend on surface parameters. *Nature* **417**, 308-311.

Bray, D. and Chapman, K. (1985). Analysis of microspike movements on the neuronal growth cone. *J. Neurosci.* **5**, 3204-3213.

Bray, D. and Hollenbeck, P. J. (1988). Growth cone motility and guidance. *Annu. Rev. Cell Biol.* **4**, 43-61.

Bray, D., Thomas, C. and Shaw, G. (1978). Growth cone formation in cultures of sensory neurons. *Proc. Natl. Acad. Sci. USA* **75**, 5226-5229.

Bridgman, P. C. and Dailey, M. E. (1989). The organization of myosin and actin in rapid frozen nerve growth cones. *J. Cell Biol.* **108**, 95-109.

Chien, C. B., Rosenthal, D. E., Harris, W. A. and Holt, C. E. (1993). Navigational errors made by growth cones without filopodia in the embryonic Xenopus brain. *Neuron* **11**, 237-251.

Clark, S. E., Moss, D. J. and Bray, D. (1983). Actin polymerization and synthesis in cultured neurones. *Exp. Cell Res.* **147**, 303-314.

Dent, E. W. and Gertler, F. B. (2003). Cytoskeletal dynamics and transport in growth cone motility and axon guidance. *Neuron* **40**, 209-227.

Di Nardo, A., Cicchetti, G., Falet, H., Hartwig, J. H., Stossel, T. P. and Kwiatkowski, D. J. (2005). Arp2/3 complex-deficient mouse fibroblasts are viable and have normal leading-edge actin structure and function. *Proc. Natl. Acad. Sci. USA* **102**, 16263-16268.

Evangelista, M., Zigmond, S. and Boone, C. (2003). Formins: signaling effectors for assembly and polarization of actin filaments. *J. Cell Sci.* **116**, 2603-2611.

Forscher, P. and Smith, S. J. (1988). Actions of cytochalasins on the organization of actin filaments and microtubules in a neuronal growth cone. *J. Cell Biol.* **107**, 1505-1516.

Gallo, G. and Letourneau, P. C. (2004). Regulation of growth cone actin filaments by guidance cues. *J. Neurobiol.* **58**, 92-102.

Goldberg, D. J. and Burmeister, D. W. (1986). Stages in axon formation: observations of growth of Aplysia axons in culture using video-enhanced contrast-differential interference contrast microscopy. *J. Cell Biol.* **103**, 1921-1931.

Grzywa, E. L., Lee, A. C., Lee, G. U. and Suter, D. M. (2006). High-resolution analysis of neuronal growth cone morphology by comparative atomic force and optical microscopy. *J. Neurobiol.* **66**, 1529-1543.

Gupton, S. L., Anderson, K. L., Kole, T. P., Fischer, R. S., Ponti, A., Hitchcock-DeGregori, S. E., Danuser, G., Fowler, V. M., Wirtz, D., Hanein, D. et al. (2005). Cell migration without a lamellipodium: translation of actin dynamics into cell movement mediated by tropomyosin. *J. Cell Biol.* **168**, 619-631.

Harborth, J., Elbashir, S. M., Bechert, K., Tuschl, T. and Weber, K. (2001). Identification of essential genes in cultured mammalian cells using small interfering RNAs. *J. Cell Sci.* **114**, 4557-4565.

Harrison, R. G. (1910). The outgrowth of the nerve fiber as a mode of protoplasmic movement. *J. Exp. Zool.* **9**, 787-848.

Heidemann, S. R., Lamoureux, P. and Buxbaum, R. E. (1990). Growth cone behavior and production of traction force. *J. Cell Biol.* **111**, 1949-1957.

Henley, J. and Poo, M. M. (2004). Guiding neuronal growth cones using Ca2+ signals. *Trends Cell Biol.* **14**, 320-330.

Higgs, H. N. and Pollard, T. D. (1999). Regulation of actin polymerization by Arp2/3 complex and WASp/Scar proteins. *J. Biol. Chem.* **274**, 32531-32534.

Higgs, H. N. and Pollard, T. D. (2001). Regulation of actin filament network formation through ARP2/3 complex: activation by a diverse array of proteins. *Annu. Rev. Biochem.* **70**, 649-676.

Hinz, B., Alt, W., Johnen, C., Herzog, V. and Kaiser, H. W. (1999). Quantifying lamella dynamics of cultured cells by SACED, a new computer-assisted motion analysis. *Exp. Cell Res.* **251**, 234-243.

Kalil, K. and Dent, E. W. (2005). Touch and go: guidance cues signal to the growth cone cytoskeleton. *Curr. Opin. Neurobiol.* **15**, 521-526.

Kovar, D. R. (2006). Molecular details of formin-mediated actin assembly. *Curr. Opin. Cell Biol.* **18**, 11-17.

Landis, S. C. (1983). Neuronal growth cones. *Annu. Rev. Physiol.* **45**, 567-580.

Lewis, A. K. and Bridgman, P. C. (1992). Nerve growth cone lamellipodia contain two populations of actin filaments that differ in organization and polarity. *J. Cell Biol.* **119**, 1219-1243.

Luo, L. (2002). Actin cytoskeleton regulation in neuronal morphogenesis and structural plasticity. *Annu. Rev. Cell Dev. Biol.* **18**, 601-635.

Marsh, L. and Letourneau, P. C. (1984). Growth of neurites without filopodial or lamellipodial activity in the presence of cytochalasin B. *J. Cell Biol.* **99**, 2041-2047.

Medeiros, N. A., Burnette, D. T. and Forscher, P. (2006). Myosin II functions in actin-bundle turnover in neuronal growth cones. *Nat. Cell Biol.* **8**, 215-226.

Mullins, R. D., Heuser, J. A. and Pollard, T. D. (1998). The interaction of Arp2/3 complex with actin: nucleation, high affinity pointed end capping, and formation of branching networks of filaments. *Proc. Natl. Acad. Sci. USA* **95**, 6181-6186.

Ng, J. and Luo, L. (2004). Rho GTPases regulate axon growth through convergent and divergent signaling pathways. *Neuron* **44**, 779-793.

Nozumi, M., Nakagawa, H., Miki, H., Takenawa, T. and Miyamoto, S. (2003). Differential localization of WAVE isoforms in filopodia and lamellipodia of the neuronal growth cone. *J. Cell Sci.* **116**, 239-246.

Pantaloni, D., Boujemaa, R., Didry, D., Gounon, P. and Carlier, M. F. (2000). The Arp2/3 complex branches filament barbed ends: functional antagonism with capping proteins. *Nat. Cell Biol.* **2**, 385-391.

Pantaloni, D., Le Clainche, C. and Carlier, M. F. (2001). Mechanism of actin-based motility. *Science* **292**, 1502-1506.

Pollard, T. D. and Borisy, G. G. (2003). Cellular motility driven by assembly and disassembly of actin filaments. *Cell* **112**, 453-465.

Quinlan, M. E., Heuser, J. E., Kerkhoff, E. and Mullins, R. D. (2005). Drosophila Spire is an actin nucleation factor. *Nature* **433**, 382-388.

Rochlin, M. W., Itoh, K., Adelstein, R. S. and Bridgman, P. C. (1995). Localization of myosin II A and B isoforms in cultured neurons. *J. Cell Sci.* **108**, 3661-3670.

Rogers, S. L., Wiedemann, U., Stuurman, N. and Vale, R. D. (2003). Molecular requirements for actin-based lamella formation in Drosophila S2 cells. *J. Cell Biol.* **162**, 1079-1088.

Schumacher, N., Borawski, J. M., Leberfinger, C. B., Gessler, M. and Kerkhoff, E. (2004). Overlapping expression pattern of the actin organizers Spir-1 and formin-2 in the developing mouse nervous system and the adult brain. *Gene Expr. Patterns* **4**, 249-255.

Smith, S. J. (1988). Neuronal cytomechanics: the actin-based motility of growth cones. *Science* **242**, 708-715.

Steketee, M. B. and Tosney, K. W. (2002). Three functionally distinct adhesions in filopodia: shaft adhesions control lamellar extension. *J. Neurosci.* **22**, 8071-8083.

Strasser, G. A., Rahim, N. A., VanderWaal, K. E., Gertler, F. B. and Lanier, L. M. (2004). Arp2/3 is a negative regulator of growth cone translocation. *Neuron* **43**, 81-94.

Suter, D. M. and Forscher, P. (2000). Substrate-cytoskeletal coupling as a mechanism for the regulation of growth cone motility and guidance. *J. Neurobiol.* **44**, 97-113.

Svitkina, T. M. and Borisy, G. G. (1998). Correlative light and electron microscopy of the cytoskeleton of cultured cells. *Methods Enzymol.* **298**, 570-592.

Svitkina, T. M. and Borisy, G. G. (1999). Arp2/3 complex and actin depolymerizing factor/cofilin in dendritic organization and treadmilling of actin filament array in lamellipodia. *J. Cell Biol.* **145**, 1009-1026.

Svitkina, T. M., Verkhovsky, A. B., McQuade, K. M. and Borisy, G. G. (1997). Analysis of the actin-myosin II system in fish epidermal keratocytes: mechanism of cell body translocation. *J. Cell Biol.* **139**, 397-415.

Svitkina, T. M., Bulanova, E. A., Chaga, O. Y., Vignjevic, D. M., Kojima, S., Vasiliev, J. M. and Borisy, G. G. (2003). Mechanism of filopodia initiation by reorganization of a dendritic network. *J. Cell Biol.* **160**, 409-421.

Tosney, K. W. and Wessells, N. K. (1983). Neuronal motility: the ultrastructure of veils and microspikes correlates with their motile activities. *J. Cell Sci.* **61**, 389-411.

Wiesner, S., Helfer, E., Didry, D., Ducouret, G., Lafuma, F., Carlier, M. F. and Pantaloni, D. (2003). A biomimetic motility assay provides insight into the mechanism of actin-based motility. *J. Cell Biol.* **160**, 387-398.

Yamada, K. M., Spooner, B. S. and Wessells, N. K. (1970). Axon growth: roles of microfilaments and microtubules. *Proc. Natl. Acad. Sci. USA* **66**, 1206-1212.

Yamada, K. M., Spooner, B. S. and Wessells, N. K. (1971). Ultrastructure and function of growth cones and axons of cultured nerve cells. *J. Cell Biol.* **49**, 614-635.

Yamaguchi, H., Lorenz, M., Kempiak, S., Sarmiento, C., Coniglio, S., Symons, M., Segall, J., Eddy, R., Miki, H., Takenawa, T. et al. (2005). Molecular mechanisms of invadopodium formation: the role of the N-WASP-Arp2/3 complex pathway and cofilin. *J. Cell Biol.* **168**, 441-452.

Zand, M. S. and Albrecht-Buehler, G. (1989). What structures, besides adhesions, prevent spread cells from rounding up? *Cell Motil. Cytoskeleton* **13**, 195-211.

Zigmond, S. H. (2004). Formin-induced nucleation of actin filaments. *Curr. Opin. Cell Biol.* **16**, 99-105.